

The $T_{cc} = DD^*$ molecular state

D. Janc¹ and M. Rosina^{1,2}

¹ *Jožef Stefan Institute, Jamova 39, P.O. Box 3000, SI-1001 Ljubljana, Slovenia*

² *Faculty of Mathematics and Physics, University of Ljubljana*

Abstract

We show that the molecule-like configuration of DD^* enables weak binding even in the case of the Bhaduri or Grenoble AL1 interaction. Three-body forces may increase the binding and strengthen the cc diquark configuration. As a signature we propose the branching ratio between radiative and pionic decay.

1 Introduction

The motivation to study tetraquarks (also called dimesons) comes from our curiosity whether we can extrapolate our understanding of mesons and baryons (in terms of quark models) to two-hadron systems. Dimesons are simpler than dibaryons (or nuclear forces) since they represent a four-body rather than a six-body system. Heavy dimesons are cleaner than light ones since nonrelativistic parametrisation and treatment are more justified and since they are likely to be longlived. Therefore in this paper we study double heavy tetraquarks as prototypes.

However, the question arises whether there is a signature of tetraquarks (dimesons) which could clearly distinguish their decay from the decay of two independent mesons. Consider the analogy. The mass of the neutron is 1.3 MeV larger than the mass of the proton, making the neutron unstable against the weak interaction and results in the $n \rightarrow p e^- \bar{\nu}_e$ decay. But when the neutron is bound in the deuteron with a binding energy of -2.23 MeV, the decay is kinematically forbidden and the neutron becomes stable. If we replace the two baryons in the deuteron with two mesons we obtain the dimeson. When one of the mesons is a vector meson, its dominant decay mode in the case of weak binding would be the radiative decay $\bar{B}^* \rightarrow \bar{B}\gamma$, or in the system of the D mesons $D^* \rightarrow D\gamma$, as well as the strong decay $D^* \rightarrow D\pi$. The $\bar{B}^*\bar{B}$ dimeson, however, is probably bound strongly enough so that radiative decay becomes energetically forbidden [1, 2, 3] and it can decay only weakly. The binding of the D^*D dimeson is expected to be much weaker, but it might still be stable against strong interaction so as to decay only electromagnetically, or, at least, the strong decay might be considerably suppressed. The dramatic change of the decay modes and lifetime of vector mesons can serve as a tool for detecting tetraquarks with nonzero total spin. This effect would be very helpful in situations where the binding energy is small compared to experimental errors so that the detection of the tetraquark from the invariant mass of final particles could not distinguish between events where the two initial mesons were either free or weakly bound before the decay.

In this study we consider tetraquarks made up of the same type of mesons, namely DD^* and $\bar{B}\bar{B}^*$ tetraquarks with quantum numbers $I = 0, S = 1, P = +1$, since they are the best candidates for binding with respect to the DD^* ($\bar{B}\bar{B}^*$) threshold, as was already noted previously [1, 2, 3]. Such states cannot decay strongly or electromagnetically into two \bar{B} or two D mesons in the S wave due to angular momentum conservation nor in the P wave due to parity conservation.

There are two extreme spatial configurations of quarks in a tetraquark. The first configuration which we call *atomic* is similar to $\bar{\Lambda}_b$, with a compact bb diquark instead of \bar{b} , around which the light antiquarks are in a similar state as in the $\bar{\Lambda}_b$ baryon. The second configuration which we

call *molecular* is deuteron-like, where two heavy quarks are well separated and the light antiquarks are bound to them similarly as in the case of free mesons. These configurations are more likely to appear in weakly bound systems. It has been shown that nonrelativistic potential models give rise to *atomic* structure for the $\bar{B}\bar{B}^*$ tetraquark [1, 2]. We use the $\bar{B}\bar{B}^*$ system as a benchmark against which we compare other tetraquarks.

In Sect. 2 we repeat calculations of the $\bar{B}\bar{B}^*$ tetraquark with the Bhaduri potential [4] and also with the AL1 potential [5] which due to the additional mass-dependent smearing of the spin-spin interaction gives a better description of meson spectroscopy. We then present results for the DD^* tetraquark, which is on the verge of being either bound or a resonant state, depending on the effective potential used in the calculations. We show that its structure is *molecular*, but with the introduction of the three-body force (Sect. 3) it can become *atomic*. The fact that this system is so close to the $D + D^*$ threshold makes it very sensitive to the details of the effective interaction and therefore a promising candidate for studying the nature of the effective interaction between constituent quarks in nonrelativistic potential models. The estimated production rate is not high but tolerable. Due to the strong influence of weak binding on the decay channels, it presents a very interesting experimental situation (Sect. 4).

2 Bound states of heavy tetraquarks

The energies of various tetraquarks were already calculated in the harmonic oscillator basis [2] where it was found that only two tetraquark systems have their energy lower than the two-free-meson threshold, namely $bb\bar{u}\bar{d}$ ($I=0, J=1$) which we denote as T_{bb} and $bb\bar{s}\bar{u}$ or $bb\bar{s}\bar{d}$ ($I=1/2, J=1$), while $bc\bar{s}\bar{u}$ or $bb\bar{s}\bar{d}$ ($I=1/2, J=1$) lies on the threshold. For deeply bound states, these results should be very accurate but since this basis cannot accommodate asymptotic states of two free mesons, there is an open question whether weakly bound states of two mesons might not have been missed.

In our work we use an expansion in the basis proposed by [3] which is described in Appendix A. There are three different sets of internal coordinates. The first one (Fig.10 a)) is convenient for expansion of those strongly correlated and deeply bound tetraquarks where we expect the *atomic* structure in which the diquark in T_{QQ} formed by two heavy quarks plays a similar role as the heavy b antiquark in the Λ_b baryon, while the light quarks in both systems are in the same radial, spin, colour and isospin configurations. The second and third sets from Fig. 10 represent the direct and exchange meson-meson channels. These configurations are needed to build up the basis for the two free mesons - the threshold state, and are also of crucial importance for searching for weakly bound tetraquarks where the molecular structure would be dominant.

We search for eigenstates of our Hamiltonian using the variational method, applying a general diagonalization of the Hamiltonian (Appendix 2) spanned by the nonorthogonal basis functions constructed in Appendix 1. We built the basis functions step by step by adding the best configurations from Fig. 10 with the best colour-spin configurations allowed for our quantum numbers ($IS=01$, positive parity and colour singlet), after having optimized the corresponding Gaussian widths. In order to obtain a 0.1 MeV accuracy we constructed bases in this way with up to $N_{max} = 90$ and $N_{max} = 140$ functions for the T_{bb} and T_{cc} tetraquarks, respectively (Appendix 3). These basis states can also accommodate two asymptotically free mesons if the four-body problem has no bound state.

2.1 T_{bb}

First we test our method on the T_{bb} system and compare our results with Ref. [2]. In our calculations we use two one-gluon exchange potentials, the Bhaduri and AL1 potential. Their properties are described in Appendix 2. The Bhaduri potential quite successfully describes the spectroscopy of the meson, as well as baryon ground states. This is an important condition since in the tetraquarks we have both quark-quark and quark-antiquark interactions. The AL1 potential

is just an improvement of the Bhaduri potential where the smearing of the colour-magnetic term in the Hamiltonian depends on the masses of the quarks. This then results in better quality of the meson spectra.

The results obtained with the Bhaduri potential are presented in Table 1 where they are compared with results from [2]. In the last two columns are listed results for the AL1 potential. Since the harmonic oscillator basis cannot accomodate two asymptotically free mesons, one obtains a positive binding energy, as for example for spin 1, isospin 1 state.

Table 1: The mass of the T_{bb} tetraquark. Column 1: spin S, isospin I, Column 2: lowest meson-meson threshold for the Bhaduri potential, Column 3: our results, Column 4: results of ref.[2] where expansion in the harmonic oscillator basis was used, Column 5: lowest meson-meson threshold for the AL1 potential, Column 6: our results with the AL1 potential.

IS	threshold [Bh]	$N_{max}=90$ [Bh]	Ref.[2] [Bh]	threshold [AL1]	$N_{max}=90$ [AL1]
01	10650.9	10518.9	10525	10644.1	10503.9
10	10601.4	10601.4	>10642	10587.0	10587.0
11	10650.9	10650.9	10712	10644.1	10644.1

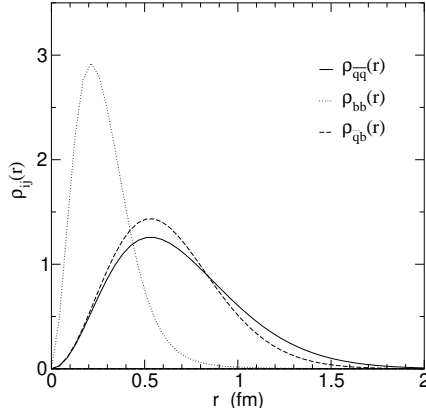


Figure 1: Probability density of two heavy quarks ρ_{bb} , of two light antiquarks $\rho_{\bar{q}\bar{q}}$ and of a light antiquark and heavy quark $\rho_{\bar{q}b}$ in T_{bb} as a function of interquark distances for the AL1 potential.

To obtain a better understanding of the T_{bb} tetraquark we now turn to the radial, spin and colour structure of this system. The probability densities for finding quark i and (anti)quark j at the interquark distance r_{ij} as shown in Fig. 1 is calculated via

$$\rho_{ij}(r) = \langle \psi | \delta(r - r_{ij}) | \psi \rangle.$$

The projection of this probability density on the colour triplet states $|\bar{3}_{12}3_{34}\rangle_C$ is

$$\rho_{ij}^{trip.}(r) = \langle \psi | \bar{3}_{12}3_{34}\rangle_C \langle \bar{3}_{12}3_{34}|_C \delta(r - r_{ij}) | \psi \rangle,$$

and similarly for the other spin and colour projections presented in Fig. 2.

From Fig. 1 it can be seen that the probability density of two heavy b quarks is strongly localized so one can make a rough approximation in which the heavy diquark is pointlike. The average distances between a light antiquark and a heavy quark, and between a light antiquark and a light antiquark are almost the same, so the heavy diquark and the two light antiquarks form some sort of equilateral triangle which can also be seen as a Mercedes-Benz configuration.

On Fig. 2a we see that the dominant colour configuration is $|\bar{3}_{12}3_{34}\rangle_C$ where two heavy quarks are in the colour antitriplet state. The $|\bar{6}_{12}\bar{6}_{34}\rangle_C$ configuration becomes relatively important at very large distances where the absolute probability density is negligible. The ratio of these two configurations approaches 2 for large separation between two b quarks which is consistent with the fact that for large distances we have two white mesons and the octet configuration is not present. This can be seen from the decomposition of colour octet and singlet (quark-antiquark)-(quark-antiquark) states into colour sextet and triplet diquark-antidiquark states.

$$\begin{aligned}
|1_{13}1_{24}\rangle_C &= \sqrt{\frac{1}{3}}|\bar{3}_{12}3_{34}\rangle_C + \sqrt{\frac{2}{3}}|\bar{6}_{12}\bar{6}_{34}\rangle_C, \\
|8_{13}8_{24}\rangle_C &= -\sqrt{\frac{2}{3}}|\bar{3}_{12}3_{34}\rangle_C + \sqrt{\frac{1}{3}}|\bar{6}_{12}\bar{6}_{34}\rangle_C, \\
|1_{14}1_{23}\rangle_C &= -\sqrt{\frac{1}{3}}|\bar{3}_{12}3_{34}\rangle_C + \sqrt{\frac{2}{3}}|\bar{6}_{12}\bar{6}_{34}\rangle_C, \\
|8_{14}8_{23}\rangle_C &= \sqrt{\frac{2}{3}}|\bar{3}_{12}3_{34}\rangle_C + \sqrt{\frac{1}{3}}|\bar{6}_{12}\bar{6}_{34}\rangle_C.
\end{aligned}$$

Since the heavy diquark is in a spatial symmetric and colour antitriplet state, it must be due to the Pauli principle in the spin symmetric $S=1$ state. This can also be seen in Fig. 2b. In this figure the $|\bar{1}_{12}1_{34}\rangle_S$ configurations are not shown since they are three orders of magnitude smaller and can thus be neglected.

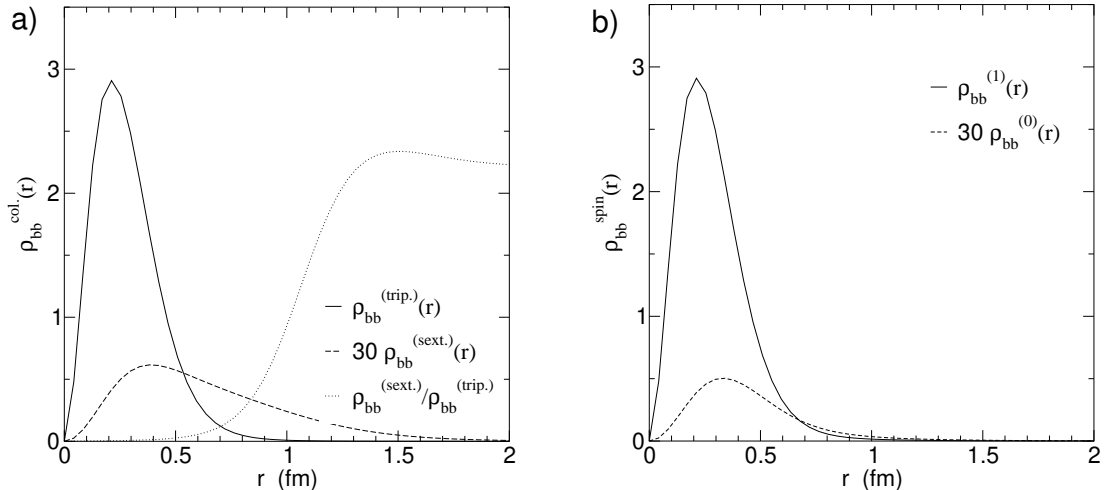


Figure 2: Results of calculations with the AL1 potential. **a)**: Probability densities ρ_{bb}^{trip} and ρ_{bb}^{sext} of the two heavy quarks projected on the colour triplet $|\bar{3}_{12}3_{34}\rangle_C$ and colour sextet states $|\bar{3}_{12}3_{34}\rangle_C$, respectively, and their ratio. **b)**: Probability density $\rho_{bb}^{(1)}$ and $\rho_{bb}^{(0)}$ of the two heavy quarks projected on the spin 1 states $|\bar{1}_{12}0_{34}\rangle_S$ and spin 0 states $|\bar{0}_{12}1_{34}\rangle_S$, respectively.

We showed that the T_{bb} tetraquark has an *atomic* $\bar{\Lambda}_b$ -like structure where the heavy diquark in the colour antitriplet state can be approximated with a heavy antiquark \bar{b} , while the light antiquarks are in isospin 0 and spin 0 state just like in $\bar{\Lambda}_b$ baryons. This then justifies the assumptions made in [1] where the binding energy was phenomenologically estimated to be -134 MeV for the AL1 potential and -139 MeV for the Bhaduri potential, which is close to the detailed calculations presented here. With its Λ_b -like structure T_{bb} cannot distinguish between one-gluon [4], [5] or one-Goldstone boson exchange [6] since in both cases the spin dependent interaction between light quarks is strongly attractive. Because of such a dominant colour triplet-triplet and radial Mercedes-Benz structure of the tetraquark, the introduction of a weak colour dependent three-body

interaction would only shift the masses of the tetraquark and not produce any significant changes in the wave function, similarly as in the baryon sector. This then makes the T_{bb} tetraquark unsuitable for studying the influence of the three-body interaction, since its effect can be compensated by a reparametrization of parameters in the two-body potential or constituent quark masses.

There are also experimental problems with the T_{bb} tetraquark. The only promising production mechanism – double two-gluon fusion ($g + g \rightarrow b + \bar{b}$)² – gives a very small production rate of about 5 events per hour at LHC [7], [8]. Moreover, since T_{bb} is below the total mass of two \bar{B} mesons, it can decay only weakly and thus has no characteristic decay different from separate \bar{B} decays. This then also makes the T_{bb} tetraquark unpromising from the experimental point of view.

2.2 T_{cc}

The T_{cc} tetraquark is much more promising than the T_{bb} tetraquark. It can be more easily produced and detected (Sect. 4) and we shall see that it is more discriminating between different binding mechanisms.

With the expansion of the tetraquark wave function in the harmonic oscillator basis one cannot find any bound state for the T_{cc} system with the Bhaduri potential. But as mentioned in the previous subsection, this can also be due to the fact that this method can miss weakly bound states. And this is exactly what happened as one can see from Table 2 where our results for the Bhaduri and the AL1 potential are presented. With both potentials, a weakly bound state does appear.

Table 2: The mass of the T_{cc} ($S=1, I=0$) tetraquark. Column 1: type of potential, Column 2: lowest meson-meson threshold for a given potential, Column 3: our results, Column 4: results of ref.[2] where expansion in the harmonic oscillator basis was used.

	threshold	$N_{max}=140$	Ref.[2]
Bhaduri	3905.3	3904.7	3931
AL1	3878.6	3875.9	

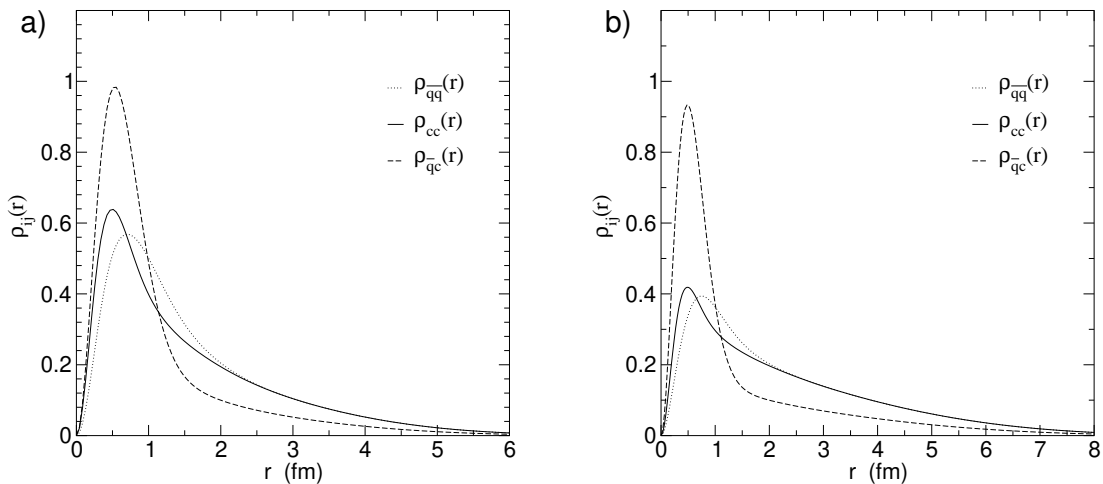


Figure 3: Probability density of the two heavy quarks ρ_{cc} , of the two light antiquarks $\rho_{q\bar{q}}$ and of a light antiquark and a heavy quark $\rho_{\bar{q}c}$ in T_{cc} as a function of the interquark distance. **a)**: results for the AL1 potential. **b)**: results for the Bhaduri potential

As in the previous subsection for the T_{bb} we now repeat the two-quark probability density analysis for the T_{cc} system. In Figs. 3 and 4 the probability densities their projections on colour and spin states as a function of interquark distance are shown.

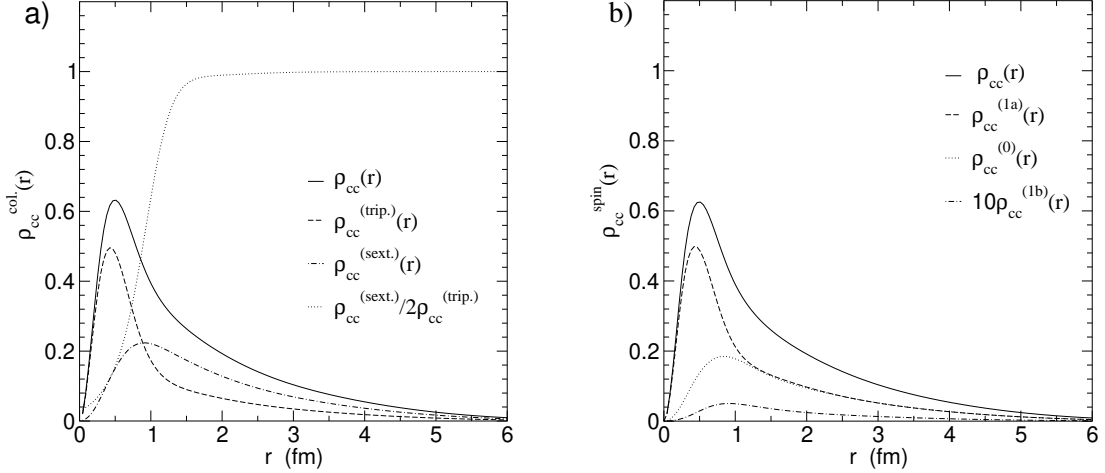


Figure 4: Results of calculations with the AL1 potential. **a)**: Probability densities ρ_{cc}^{trip} and ρ_{cc}^{sext} of the two heavy quarks as a function of interquark distance projected on the colour triplet state $|\bar{3}_{12}3_{34}\rangle_C$ and on the colour sextet state $|\bar{3}_{12}3_{34}\rangle_C$, respectively. **b)**: Probability densities $\rho_{cc}^{(1a)}$, $\rho_{cc}^{(1b)}$ and $\rho_{cc}^{(0)}$ for the two heavy quarks as a function of interquark distance projected on the spin 1 states $|1_{12}0_{34}\rangle_S$ and $|1_{12}1_{34}\rangle_S$ and on spin 0 state $|0_{12}1_{34}\rangle_S$, respectively.

We can see in Fig. 3 that the wave function between heavy quarks is much broader and has an exponential tail at large distances. If we look at the structure of the quark-quark probability density in Fig. 4a we see that at around $r \sim 1$ fm sextet configurations become larger than triplet ones and soon after the ratio of the colour configurations stabilizes at 2. This supports the picture of molecular binding of the D and D^* meson in the T_{cc} . This can be also confirmed from the results shown in Fig. 4b where at distances larger than 1 fm the probability for two heavy quarks in spin 0 and spin 1 states is equal. This follows from spin recoupling

$$|1_{13}0_{24}\rangle_S = -\sqrt{\frac{1}{2}} \left[|1_{12}1_{34}\rangle_S + \frac{1}{\sqrt{2}} (|1_{12}0_{34}\rangle_S - |0_{12}1_{34}\rangle_S) \right],$$

$$|0_{13}1_{24}\rangle_S = -\sqrt{\frac{1}{2}} \left[|1_{12}1_{34}\rangle_S - \frac{1}{\sqrt{2}} (|1_{12}0_{34}\rangle_S - |0_{12}1_{34}\rangle_S) \right].$$

If we assume that the tetraquark spin wave function is symmetric due to permutation of identical particles and thus has the form

$$|\psi\rangle \sim 1/2 (|1_{13}0_{24}\rangle_S + |0_{13}1_{24}\rangle_S) = -1/\sqrt{2} (|1_{12}0_{34}\rangle_S - |0_{12}1_{34}\rangle_S),$$

the contribution of the $|1_{12}0_{34}\rangle_S$ and of the $|0_{12}1_{34}\rangle_S$ configurations should be equal. Similar conclusion also holds, if we recouple to $|1_{14}0_{23}\rangle_S$ and $|0_{14}1_{23}\rangle_S$. All relevant spin recouplings can be found in [3].

The probability density of the light antiquarks $\rho_{\bar{q}\bar{q}}$ shows similar behaviour, while the radial dependence of the quark-antiquark probability density $\rho_{\bar{q}c}$ has a strong peak at smaller distances and a twice lower tail than the ρ_{cc} and $\rho_{\bar{q}\bar{q}}$ (Fig. 3). How this structure appears is shown in Fig. 5. Due to symmetrization of the configurations into which we expand the tetraquark wave function, the first light antiquark is bound to both heavy quarks c_1 and c_2 with equal probability. The probability density $\rho_{\bar{q}c}(r, r_{cc})$ of finding the first light antiquark at the interquark distance r from

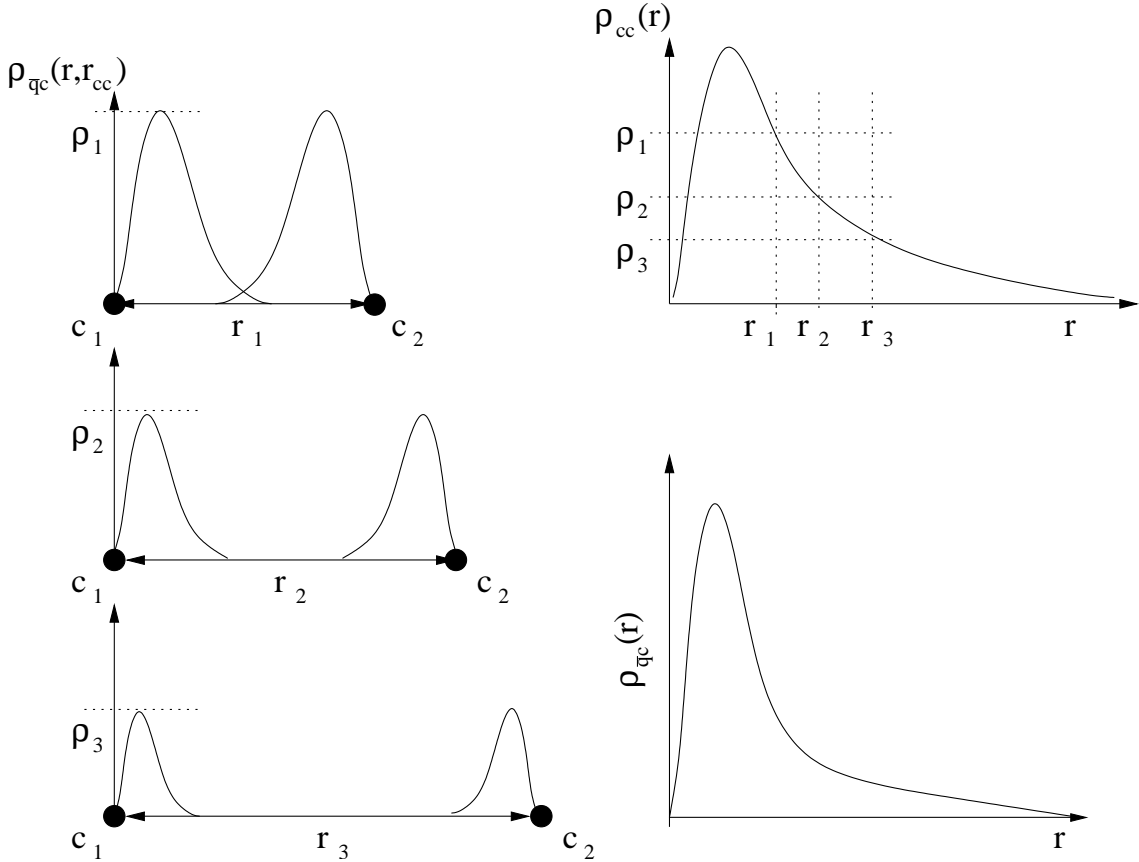


Figure 5: Decomposition of the quark-antiquark probability density $\rho_{\bar{q}c}$ (bottom right) into contributions corresponding to different distances between heavy quarks (left). The details are explained in the text.

the first heavy quark when the distance between the heavy quarks r_{cc} is r_1 , r_2 and r_3 is shown on the left hand side of Fig. 5. The heights ρ_i are proportional to the probability density of finding two heavy quarks at the interquark distance r_i , as is schematically depicted on the top right of Fig. 5. After integrating over all possible interquark positions r_i we obtain a strong peak when the light antiquark is bound to the first heavy quark c_1 and a long tail when it is bound to the second heavy quark c_2 . If we ignore the interference between these two situations which appears when r_i is smaller than the size of the free D meson, half of the probability is in the peak and the other half in the tail.

The colour and spin decomposition of the quark-antiquark probability density $\rho_{\bar{q}c}$ is shown in Fig. 6. We see that at small distances ($r < 1$ fm) where the peak is situated, the probability density is dominated by the pseudoscalar D meson $|0_{13}1_{24}\rangle$ and the vector D^* meson $|1_{13}0_{24}\rangle$. To understand the spin structure of the tail, we also present on the same graph the projection on the spin $|1_{14}0_{23}\rangle$, $|0_{14}1_{23}\rangle$ and $|1_{14}1_{23}\rangle$ states. We see that the dominance of the spin $|1_{13}1_{24}\rangle$ structure occurs due to the equal admixture of $|0_{14}1_{23}\rangle$ and $|1_{14}0_{23}\rangle$ states. From this we can conclude that there is no appreciable contribution from the D^*D^* configuration for large r . The octet colour dominance at small interquark distances is due to the formation of diquark-antidiquark structure, similar as to that in T_{bb} . But in T_{cc} this is not a dominant structure, it represents only about a third of the total probability in the case of the AL1 potential and even less for the Bhaduri potential.

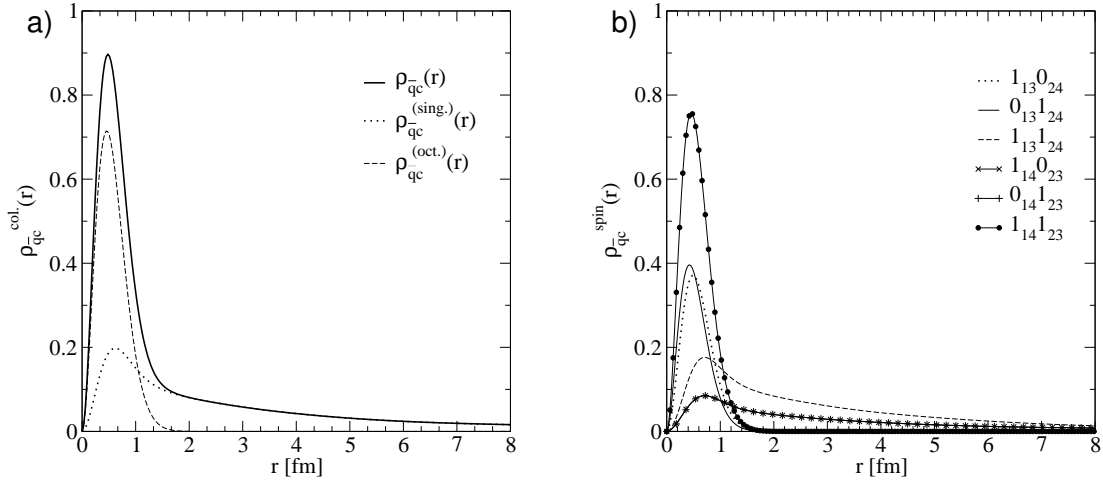


Figure 6: Results for calculations with the Bhaduri potential. **a)**: Probability densities $\rho_{\bar{q}c}^{\text{sing.}}$ and $\rho_{\bar{q}c}^{\text{oct.}}$ of the quark and antiquark projected on the colour singlet $|1_{14}1_{23}\rangle_C$ and colour octet states $|8_{14}8_{23}\rangle_C$, respectively. **b)**: Projection of Probability density $\rho_{\bar{q}c}^{(1)}$ on various spin states. The $|0_{13}1_{24}\rangle_S$ and $|1_{13}0_{24}\rangle_S$ projections are almost exactly (after renormalization) the probability densities of D and D^* mesons, respectively.

We also analysed the decrease of the tail of the probability densities from Fig. 3a. At large distances one can approximate the tetraquark as a bound state of two mesons which is described by the Schrödinger equation

$$-\frac{\hbar^2}{2m_r} \frac{d^2}{dr^2} \psi + V(r) \psi + E \psi,$$

where m_r is the reduced mass of D and D^* . Assuming that at large distances the colour wave function is singlet, the potential $V(r)$ should approach zero and thus the asymptotic behavior of ψ should be

$$\psi(r \rightarrow 0) \rightarrow \exp(-\kappa r), \quad \kappa = \sqrt{|E|m_r}/\hbar c. \quad (1)$$

This can be very clearly seen in Fig. 7 where we plotted the logarithm of the wave functions. The quark-antiquark probability density is multiplied by 2 as explained in the previous paragraph. All three interquark probability densities follow the predicted exponential decrease from Eq. 1.

3 Three-body interaction

The idea of introducing a small amount of three-body interaction into nonrelativistic potential models is not new. In the baryon sector this additional interaction can be used to better reproduce the ground state spectroscopy [5]. But generally, a slight three-body interaction cannot produce any significant changes in other baryon properties, and the desirable shift of levels can also be reproduced by modification of the parameters in the two-body potential.

Before we introduce such an interaction into the tetraquark system we shortly discuss the structure of this interaction. For the radial part we take the simplest possible radial dependence – the smeared delta function of the coordinates of the three interacting particles. Since we are working with the colour·colour type potential it is natural that also the three-body potential possesses some colour structure. The colour factor in the two-body Bhaduri or AL1 potential is proportional to the first (quadratic) Casimir operator $C^{(1)}$; $C^{(1)} = \lambda \cdot \lambda$. Following this, we introduce in the three-body

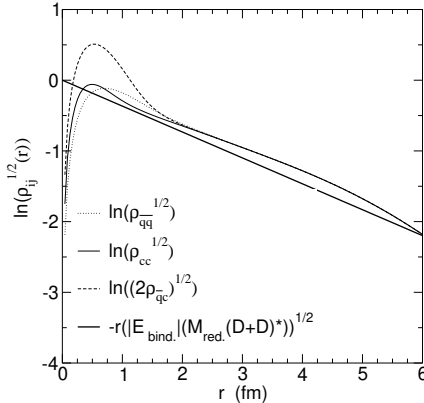


Figure 7: Logarithms of probability density as a function of interquark distances compared with the analytically expected slope

potential the second $C^{(2)}$ (cubic) Casimir operator $C^{(2)} = d^{abc} \lambda_a \cdot \lambda_b \cdot \lambda_c$. A deeper discussion of the properties that the colour dependent three-body interaction must fulfil can be found in [14], [15], [16].

It should be noted that in the baryon sector such a colour structure is irrelevant since there is only one colour singlet state and thus the colour factor is just a constant which can be included into the strength of the potential. In tetraquarks the situation is different since there are two colour singlet states: $|\bar{3}_{12}3_{34}\rangle$ and $|6_{12}\bar{6}_{34}\rangle$ (or $|1_{13}1_{24}\rangle$ and $|8_{13}8_{24}\rangle$ after recoupling). The three-body force operates differently on these two states and one can anticipate that in the case of the weak binding it can produce large changes in the structure of the tetraquark. This cannot be otherwise produced simply by reparametrization of the two-body potential, so the weakly bound tetraquarks are a very important laboratory for studying the effect of such an interaction.

The form of the three-body interaction we introduced into the tetraquark is

$$\begin{aligned} V_{q\bar{q}\bar{q}}^{3b}(\vec{r}_i, \vec{r}_j, \vec{r}_k) &= -\frac{1}{8} d^{abc} \lambda_i^a \lambda_j^b \lambda_k^{c*} U_0 \exp[-(r_{ij}^2 + r_{jk}^2 + r_{ki}^2)/r_0^2], \\ V_{q\bar{q}\bar{q}}^{3b}(\vec{r}_i, \vec{r}_j, \vec{r}_k) &= \frac{1}{8} d^{abc} \lambda_i^a \lambda_j^{b*} \lambda_k^{c*} U_0 \exp[-(r_{ij}^2 + r_{jk}^2 + r_{ki}^2)/r_0^2]. \end{aligned}$$

Here r_i is the distance of the i -th quark from the centre of the triangle formed by i -th, j -th and k -th quark, and similarly for r_j and r_k . λ_a are the Gell-Mann colour matrices and d^{abc} are the SU(3) structure constants ($\{\lambda^a, \lambda^b\} = 2d^{abc}\lambda^c$).

The diagonal matrix elements of the colour part of the three-body interaction between two quarks and an antiquark are $-5/18$ and $5/9$ for $|\bar{3}_{12}3_{34}\rangle$ and $|6_{12}\bar{6}_{34}\rangle$ colour states, respectively. If the strength of this interaction U_0 is negative it will lower the states with diquark-antidiquark configuration and increase the binding as can be seen on Fig. 8b. For a strong three-body interaction T_{cc} loses the molecular structure and the triplet-triplet colour configurations become dominant and the T_{cc} tetraquark becomes similar to T_{bb} . A drastic change in the width of the probability density can already be seen for strength $U_0 = -20$ MeV. In the baryon sector such an interaction would merely lower the states by about U_0 so it would have no dramatic effect nor would it spoil the fit to experimental data. Since the predicted energies of ground state baryons for the Bhaduri and AL1 potential are above the experimental values, this is actually a desirable feature. The dependence of the mass of the T_{cc} tetraquark on the strength of the potential U_0 and on the smearing of this potential is shown in Fig. 8b. One can see that for large smearing the mass of the tetraquark is shifted by about $4\frac{5}{18}U_0$ in agreement with the dominance of the triplet-triplet colour configuration in this state.

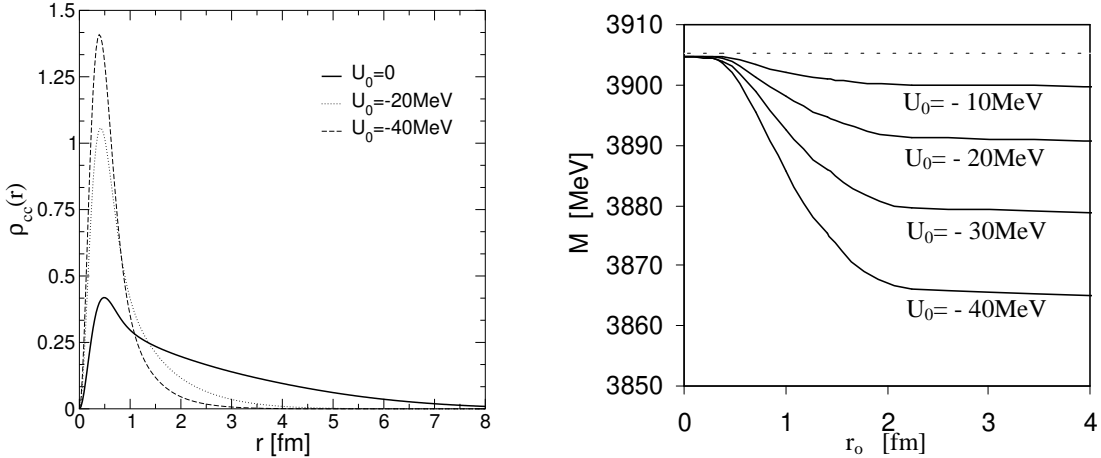


Figure 8: **a)**: Probability density between two c quarks in the T_{cc} tetraquark as a function of interquark distance for three different values of the strength of the three-body potential. **b)**: Mass of the T_{cc} tetraquark as a function of the smearing parameter in the three-body interaction for four different strengths of the three-body potential.

4 Production and detection of T_{cc}

We shall focus only on the possibility of detecting the T_{cc} tetraquark, since even at LHC the production of the T_{bb} tetraquark would be below the rate where one could hope to detect it.

Since double charmed baryons were probably detected at SELEX [9] one can expect that if the T_{cc} is bound, it was also produced there, with a production rate about ten times smaller than double charmed baryons. This estimate is based on the fact that a heavy quark gets dressed with a light antiquark into a heavy meson with a probability of roughly 0.9, and with a probability of 0.1 it combines with two light quarks into a Λ baryon [10]. But since SELEX found, with their cuts, only fifty candidates for double charmed baryons, the statistics for detecting double charmed tetraquarks should be improved. Another experiment where one might look for T_{cc} could be provided by LHC where one can estimate the production rate as large as 10^4 events/hour [11].

However, the T_{cc} tetraquark has a molecular structure in which the mesonic wave function is not strongly influenced by the other meson. The large mean square radius of the T_{cc} tetraquark has consequences for the production mechanism. It is no longer required that the two c quarks come close to produce first a diquark which then gets dressed by light antiquarks. This can give a larger production rate at SELEX than estimated above. This also makes machines like the RHIC ion collider [12] interesting candidates for searching for tetraquarks.

There is also an interesting possibility of production and detection of the T_{cc} tetraquark in B-factories. Belle [17] has reported a measurement of double charm production in e^+e^- annihilation at $\sqrt{s} = 10.6$ GeV and found that

$$\sigma(e^+e^- \rightarrow J/\psi c\bar{c}) \sim 1\text{pb},$$

which corresponds to about 2000 events. Since the total mass of four D mesons is close to the c.m. energy, the c quarks created in this process have small relative momentum which is very important in the T_{cc} production.

The main problem with detection of the weakly bound T_{cc} tetraquark is how to distinguish the pion or photon emitted by the decay of the free D^* meson from the one emitted by the D^* meson bound inside the tetraquark. We can exploit the fact that the phase space for $D^* \rightarrow D + \pi$ decay is very small. Note that $m_{D^{*+}} - m_{D^+} - m_{\pi^0} = 5.6 \pm 0.1$ MeV, $m_{D^{*0}} - m_{D^0} - m_{\pi^0} = 7.1 \pm 0.1$ MeV, $m_{D^{*+}} - m_{D^0} - m_{\pi^+} = 5.87 \pm 0.02$ MeV. This has a strong impact on the branching

ratio between radiative and hadronic decay. Since the D^* meson inside the tetraquark is not significantly influenced by the other D meson (Fig. 5) in the tetraquark, we expect that the partial width for the magnetic dipole $M1$ transition would be very close to the width of the free meson while the width for hadronic $D^* \rightarrow D + \pi$ decay will decrease with stronger binding and will become energetically forbidden below the $D + \pi$ threshold. The hadronic decay of the T_{cc} tetraquark is a three-body decay which is commonly represented by the Dalitz plot.

Let us assume that the T_{cc} tetraquark is below the $D + D^*$ threshold but above the $D + D + \gamma$ and $D + D + \pi$ as was the case in our nonrelativistic potential models. Then the partial decay rate for the $T_{cc} \rightarrow D + D + \pi$ is given by

$$d\Gamma = \frac{1}{(2\pi)^3} \frac{1}{32M^3} \overline{|\mathcal{M}|^2} dm_{12}^2 dm_{23}^2 \quad (2)$$

where particles 1 and 2 are two final D mesons and particle 3 is a π emerging from the decaying tetraquark. Here $m_{12}^2 = (p_D + p_D)^2$ and $m_{23}^2 = (p_D + p_\pi)^2$ and M is the mass of the tetraquark. Since the total masses of the $D^* + D$ and $2D + \pi$ are so close there is a strong isospin violation in the decay which cannot be reproduced with the Bhaduri or AL1 potential where the D^* and the D isospin doublets are degenerate. We shall not try to modify the interaction to accomodate the dependence of the decay on the isospin of the particles, but we shall rather work with the experimental masses taken from the PDG [18]. The allowed region of integration over dm_{12}^2 and dm_{23}^2 for three different binding energies is plotted on Fig. 9a. If we assume $\overline{|\mathcal{M}|^2}$ is constant, which is very plausible in our case, the allowed region will be uniformly populated with experimental events so that the measured partial decay rate Γ will be proportional to the kinematically allowed area from Fig. 9a. The dependence of this area I as a function of the binding energy of the tetraquark is shown on Fig. 9b.

Up to now, we have discussed only true bound states, but the T_{cc} tetraquark can also be a resonant state above the $D + D^*$ threshold. Then if the resonance is situated near the threshold, beside the $T_{cc} \rightarrow D + D^*$ decay there will still be a significant fraction of hadronic $T_{cc} \rightarrow D + D + \pi$ decays. This region of positive binding energy is not presented in Fig. 9. But one can see that in a similar manner as in the case of weakly bound tetraquarks the low-lying resonant state can be identified from the Dalitz plot.

Table 3: Mean distance between two heavy quarks $\langle r_{cc} \rangle$ in the T_{cc} tetraquark and the value of the centrifugal potential for $L=2$ state for the Bhaduri and the AL1 potential.

	$\langle r_{cc} \rangle$	$(\hbar^2 L(L+1)/2M_{red}) \langle 1/r_{cc}^2 \rangle$
Bhaduri (L=2)	2.4 fm	174 MeV
AL1 (L=2)	1.6 fm	232 MeV

As a remark, we present an alternative way of detecting the weakly bound tetraquark. Since the mean radius of the tetraquark is large, as one can see from Table 3, the centrifugal barrier for the $L=0 \rightarrow L=2$ transition is comparable with the available energy in the D^* decay, so there is also a possibility of the electric quadrupole transition $E2$. This is a two pion exchange process which is beyond the scope of the potential model used here.

5 Conclusions

We have shown that in popular nonrelativistic potential models the T_{cc} tetraquark is bound against the DD^* threshold and that it has a *molecular* structure. Therefore the approximation based on the assumption of the *atomic* $\bar{\Lambda}_b$ -like structure which suggests that the system is not bound [1] is not valid. This dramatically different situation as compared with the T_{bb} tetraquark makes the T_{cc} tetraquark an interesting laboratory for more profound studies of the nature of the interactions

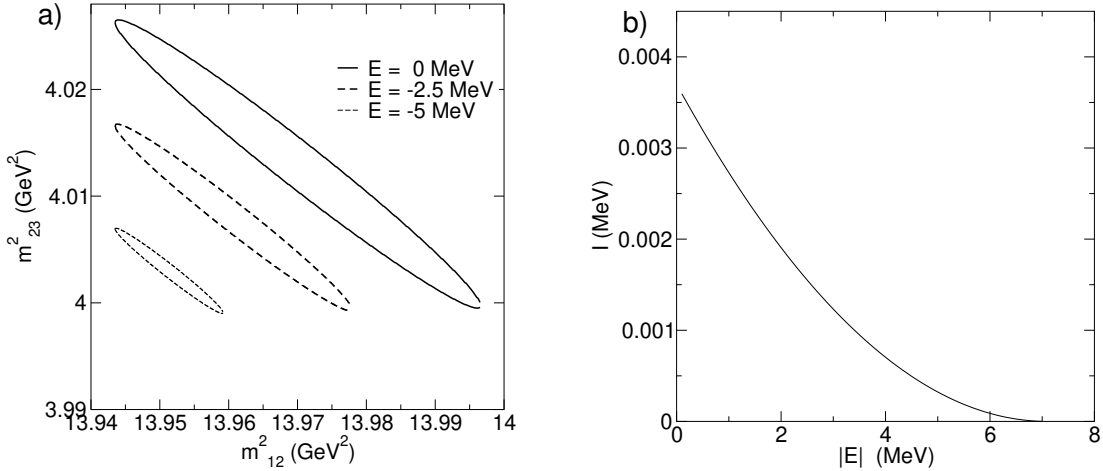


Figure 9: **a)**: Dalitz plot, **b)**: Integrated Dalitz plot

between quarks, since such a weakly bound system is more sensitive to the detailed features of the interaction.

As a signature for the $T_{cc} = DD^*$ tetraquark one might exploit the very small phase space of the $D^* \rightarrow D\pi$ decay which is very sensitive to the binding energy of D^* to D .

We did not study in detail the $cc\bar{s}\bar{u}$ tetraquark since it has a lower threshold, $D_s D$ rather than $D_s D^*$ or $D_s^* D$, and it is not likely to be bound.

Acknowledgement. The authors would like to acknowledge the encouragement by Jean-Marc Richard to look whether the DD^* system might be bound after all. Acknowledgment is also due to the collaboration with Daniele Treleani and Alessio Del Fabbro on questions of production of the T_{bb} and T_{cc} tetraquarks.

This work was supported by the Ministry of Education, Science and Sport of the Republic of Slovenia.

6 Appendix

6.1 Configurations

We express the orbital part of the tetraquark wave function in terms of Gaussians. The coordinate systems used here are shown in Fig. 10. The transformation between various coordinate systems and some details about the calculation of the kinetic and potential matrix elements are given in [3].

The most general form for the ground state of the tetraquark ($L=0$) can be expanded in any of the three configurations given in Fig. 10

$$R = \sum_n C_n K_r(C_{ij}^n), \quad C_{ij}^n = C_{ji}^n, \quad r = 1 \text{ or } 2 \text{ or } 3.$$

So far it looks as if not all coordinate systems were needed, but in numerical calculation it is convenient to limit the test functions to those in which $C_{ij} = 0$ if $i \neq j$. With this we reduce our problem of optimization of 6 parameters C_{ij} into three optimizations ($r = 1, 2, 3$) of 3 parameters $C_{ii} = \{c_1, c_2, c_3\}$. Though this somewhat restricts our Hilbert space we still expect that it would not have any significant effect on the calculation of the ground state, because by using all three configurations from Fig. 10 we can have nonzero relative angular momentum between two quarks

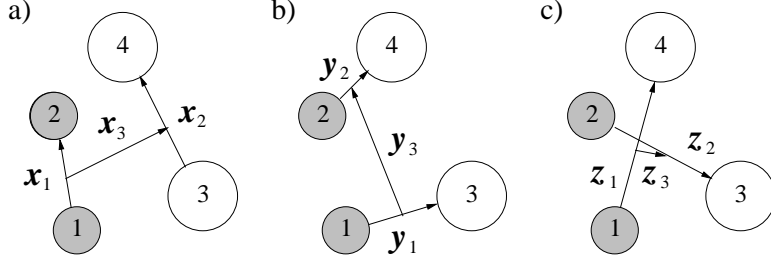


Figure 10: Two quarks (dashed circles) and two antiquarks (empty circles) in three different relative coordinate systems. The orbital wave function is then a gaussian function of relative coordinates. a) diquark-antidiquark: $K_1(C_{ij}) = \exp(-\mathbf{x}_i C_{ij} \mathbf{x}_j)$, b) direct channel: $K_2(C_{ij}) = \exp(-\mathbf{y}_i C_{ij} \mathbf{y}_j)$, c) exchange channel: $K_3(C_{ij}) = \exp(-\mathbf{z}_i C_{ij} \mathbf{z}_j)$.

l_{12} or two antiquarks l_{34} by using the systems b) and c) but still keep the total angular momentum zero. The orbital part of the wave function has thus the form

$$R = \sum_n C_n K_r(c_1^n, c_2^n, c_3^n), \quad r = 1, 2, 3.$$

The tetraquark wave function must posses correct symmetry against the permutation of the two quarks $P(1, 2)$ or antiquarks $P(3, 4)$. The effect of these permutations on relative coordinates are

$$\begin{aligned} P(1, 2)[K_1(c_i)] &= K_1(c_i), & P(3, 4)[K_1(c_i)] &= K_1(c_i), \\ P(1, 2)[K_2(c_1, c_2, c_3)] &= K_3(c_2, c_1, c_3), & P(3, 4)[K_2(c_i)] &= K_3(c_i), \\ P(1, 2)[K_3(c_1, c_2, c_3)] &= K_2(c_2, c_1, c_3), & P(3, 4)[K_3(c_i)] &= K_2(c_i). \end{aligned}$$

We see that if $c_1 \neq c_2$ the configuration K_2 and K_3 loose symmetry properties with respect to permutations of the heavy quarks. To obtain functions with good permutation symmetry we make linear combinations of configurations. For shorter notation we introduce $K_i(c_2, c_1, c_3) = \tilde{K}_i(c_1, c_2, c_3)$

$$\begin{aligned} R_1(c_i) &= K_1(c_i), \\ R_2(c_i) &= K_2(c_i) + K_3(c_i) + \tilde{K}_2(c_i) + \tilde{K}_3(c_i), \\ R_3(c_i) &= K_2(c_i) - K_3(c_i) + \tilde{K}_2(c_i) - \tilde{K}_3(c_i), \\ R_4(c_i) &= K_2(c_i) - K_3(c_i) - \tilde{K}_2(c_i) + \tilde{K}_3(c_i), \\ R_5(c_i) &= K_2(c_i) + K_3(c_i) - \tilde{K}_2(c_i) - \tilde{K}_3(c_i). \end{aligned}$$

The effect of permutation of identical (anti)quarks is then

$$\begin{aligned} P(12)[R_1(c_i)] &= P(34)[R_1(c_i)] = R_1(c_i), \\ P(12)[R_2(c_i)] &= P(34)[R_2(c_i)] = R_2(c_i), \\ P(12)[R_3(c_i)] &= P(34)[R_3(c_i)] = -R_3(c_i), \\ P(12)[R_4(c_i)] &= -P(34)[R_4(c_i)] = R_4(c_i), \\ P(12)[R_5(c_i)] &= -P(34)[R_5(c_i)] = -R_5(c_i). \end{aligned}$$

In the spin space of four quarks we have three different spin 1 representations. Most suitable basis for studying permutation properties is obtained by coupling the quarks into a diquark and

antiquarks into a antidiquark. The three basis states are then

$$|1_{12}, 0_{34}\rangle, \quad |0_{12}, 1_{34}\rangle, \quad |1_{12}, 1_{34}\rangle, \quad (3)$$

and the permutation of identical particles on this states gives

$$\begin{aligned} P(12)[|1_{12}, 0_{34}\rangle] &= |1_{12}, 0_{34}\rangle, & P(34)[|1_{12}, 0_{34}\rangle] &= -|1_{12}, 0_{34}\rangle, \\ P(12)[|0_{12}, 1_{34}\rangle] &= -|0_{12}, 1_{34}\rangle, & P(34)[|0_{12}, 1_{34}\rangle] &= |0_{12}, 1_{34}\rangle, \\ P(12)[|1_{12}, 1_{34}\rangle] &= |1_{12}, 1_{34}\rangle, & P(34)[|1_{12}, 1_{34}\rangle] &= |1_{12}, 1_{34}\rangle. \end{aligned}$$

In the colour space there are two different colour singlet representations which in the diquark-antidiquark basis can be expressed as

$$|\bar{3}_{12}, 3_{34}\rangle, \quad |6_{12}, \bar{6}_{34}\rangle, \quad (4)$$

and we have

$$\begin{aligned} P(12)[|\bar{3}_{12}, 3_{34}\rangle] &= -|\bar{3}_{12}, 3_{34}\rangle, & P(34)[|\bar{3}_{12}, 3_{34}\rangle] &= -|\bar{3}_{12}, 3_{34}\rangle, \\ P(12)[|6_{12}, \bar{6}_{34}\rangle] &= |6_{12}, \bar{6}_{34}\rangle, & P(34)[|6_{12}, \bar{6}_{34}\rangle] &= |6_{12}, \bar{6}_{34}\rangle. \end{aligned}$$

From the original three spatial configuration shown in Fig. 10, the three spin configurations given in Eq.(3) and two colour configuration of Eq.(4) one can build up $3 \cdot 3 \cdot 2 = 18$ function. Eight of them are antisymmetric with respect to exchange of heavy quarks and symmetric (isospin 0) with respect to exchange of light antiquarks.

$$\begin{aligned} \psi_1 &= R_1(c_i)|\bar{3}_{12}3_{34}\rangle_C|1_{12}0_{34}\rangle_S, & \psi_2 &= R_1(c_i)|6_{12}\bar{6}_{34}\rangle_C|0_{12}1_{34}\rangle_S, \\ \psi_3 &= R_2(c_i)|\bar{3}_{12}3_{34}\rangle_C|1_{12}0_{34}\rangle_S, & \psi_4 &= R_2(c_i)|6_{12}\bar{6}_{34}\rangle_C|0_{12}1_{34}\rangle_S, \\ \psi_5 &= R_3(c_i)|6_{12}\bar{6}_{34}\rangle_C|1_{12}0_{34}\rangle_S, & \psi_6 &= R_3(c_i)|\bar{3}_{12}3_{34}\rangle_C|0_{12}1_{34}\rangle_S, \\ \psi_7 &= R_4(c_i)|\bar{3}_{12}3_{34}\rangle_C|1_{12}1_{34}\rangle_S, & \psi_8 &= R_5(c_i)|6_{12}\bar{6}_{34}\rangle_C|1_{12}1_{34}\rangle_S. \end{aligned}$$

For better description of weakly bound states we also add additional configurations which cannot be decomposed into a simple product of orbital, colour and spin parts.

$$\begin{aligned} \psi_9 &= \left((K_2(c_i) + \tilde{K}_2(c_i))|1_{13}1_{24}\rangle_C + (K_3(c_i) + \tilde{K}_3(c_i))|1_{14}1_{23}\rangle_C \right) |0_{12}1_{34}\rangle_S, \\ \psi_{10} &= \left((K_2(c_i) + \tilde{K}_2(c_i))|1_{13}1_{24}\rangle_C - (K_3(c_i) + \tilde{K}_3(c_i))|1_{14}1_{23}\rangle_C \right) |1_{12}0_{34}\rangle_S, \\ \psi_{11} &= (K_2(c_i) - \tilde{K}_2(c_i))|1_{13}1_{24}\rangle_C|0_{13}1_{24}\rangle_S + (K_3(c_i) - \tilde{K}_3(c_i))|1_{14}1_{23}\rangle_C|0_{14}1_{24}\rangle_S, \\ \psi_{12} &= (K_2(c_i) - \tilde{K}_2(c_i))|1_{13}1_{24}\rangle_C|1_{13}0_{24}\rangle_S + (K_3(c_i) - \tilde{K}_3(c_i))|1_{14}1_{23}\rangle_C|1_{14}0_{23}\rangle_S, \\ \psi_{13} &= (K_2(c_i) - \tilde{K}_2(c_i))|1_{13}1_{24}\rangle_C|1_{13}1_{24}\rangle_S + (K_3(c_i) - \tilde{K}_3(c_i))|1_{14}1_{23}\rangle_C|1_{14}1_{23}\rangle_S. \end{aligned}$$

It is obvious that these configurations also respect permutation symmetry.

If we have a strong quark mass asymmetry we expect diquark-antidiquark clustering [3], so that the first coordinate system on Fig. 10 is more suitable and the dominant colour configuration has the diquark in antitriplet and the antidiquark in triplet colour state. On the other hand, if the binding is weak, the direct and exchange meson-meson channels are more adequate and the important configuration has singlet-singlet colour structure.

6.2 Potential models

For solving Schrödinger equation in nondiagonal basis we use general diagonalization of the Hamiltonian

$$\langle \psi_k^m | H | \psi_l^n \rangle = \langle \psi_k^m | W_k | \psi_l^n \rangle + \langle \psi_k^m | \sum_{\substack{i=1..3; \\ j=i+1..4}} V_{ij} | \psi_l^n \rangle, \quad (5)$$

$$k, l = 1, ..13; \quad m, n = 1, ..N_{max};$$

where $|\psi_k^m\rangle$ is the m-th basis function (See Appendix 3) and N_{max} is the dimension of the basis. The kinetic energy operator written in the basis a) of Fig.10 has the form

$$\langle \psi_k^m | W_k | \psi_l^n \rangle = -6 \langle \psi_k^m | \psi_l^n \rangle \text{Tr} \left[(C^m + C^n)^{-1} C^m T C^n \right],$$

$$T = \frac{\hbar^2 c^2}{2} \begin{pmatrix} \frac{m_1+m_2}{2m_1m_2} & 0 & \frac{m_2-m_1}{2\sqrt{2}m_1m_2} \\ 0 & \frac{m_3+m_4}{2m_3m_4} & \frac{m_3-m_4}{2\sqrt{2}m_3m_4} \\ \frac{m_2-m_1}{2\sqrt{2}m_1m_2} & \frac{m_3-m_4}{2\sqrt{2}m_3m_4} & \frac{1}{4} \sum_{i=1}^4 \frac{1}{m_i} \end{pmatrix}.$$

We tested two different potentials. First one was proposed by Bhaduri and collaborators [4] and the improved one proposed by Silvestre-Brac and Semay [5] which we will denote by AL1 potential.

- Bhaduri potential:

$$V_{ij}^B = -\frac{\lambda_i^C}{2} \cdot \frac{\lambda_j^C}{2} \left(U_0 + \frac{\alpha}{r_{ij}} + \beta r_{ij} + \alpha \frac{\hbar^2}{m_i m_j c^2} \frac{e^{-r_{ij}/r_0}}{r_0^2 r_{ij}} \sigma_i \cdot \sigma_j \right), \quad (6)$$

$$r_{ij} = |\vec{r}_i - \vec{r}_j|;$$

$$\begin{aligned} m_b &= 5259 \text{ MeV}, & m_c &= 1870 \text{ MeV}, \\ m_s &= 600 \text{ MeV}, & m_u &= m_d = 337 \text{ MeV}, \\ U_0 &= 685 \text{ MeV}, & \alpha &= 77 \text{ MeVfm}, \\ \beta &= 706.95 \text{ MeV/fm}, & r_0 &= 0.4545 \text{ fm}. \end{aligned}$$

- AL1 potential

$$V_{ij}^{AL1} = -\frac{\lambda_i^C}{2} \cdot \frac{\lambda_j^C}{2} \left(U_0 + \frac{\alpha}{r_{ij}} + \beta r_{ij} + \tilde{\alpha} \frac{2\pi\hbar^2}{3m_i m_j c^2} \frac{e^{-r_{ij}^2/r_0^2}}{\pi^{3/2} r_0^3} \sigma_i \cdot \sigma_j \right), \quad (7)$$

$$r_0(m_i, m_j) = A \left(\frac{m_i + m_j}{2m_i m_j} \right)^B, \quad r_{ij} = |\vec{r}_i - \vec{r}_j|;$$

$$\begin{aligned} m_b &= 5227 \text{ MeV}, & m_c &= 1836 \text{ MeV}, & A &= 1.6553 \text{ GeV}^{B-1}, \\ m_s &= 577 \text{ MeV}, & m_u &= m_d = 315 \text{ MeV}, & B &= 0.2204, \\ U_0 &= 624.075 \text{ MeV}, & \alpha &= 74.895 \text{ MeVfm}, \\ \beta &= 629.315 \text{ MeV/fm}, & \tilde{\alpha} &= 274.948 \text{ MeVfm}. \end{aligned}$$

6.3 Numerics

We solve our four body problem by diagonalization of the Hamiltonian in a space spanned by Gaussian function. We built our basis step by step so that at each step all configurations $|\psi_\alpha\rangle$ ($\alpha = 1, \dots, 13$) are tested and parameters c_i are optimized. We then took the best configuration as the next base state. This procedure is very similar to the stochastic variational approach [19]. The main reason for using gaussian basis is that all matrix elements can be evaluated analytically. We

were very careful that the basis states are linearly independent so that the eigenvalues of the overlap matrix $\langle \psi_\alpha | \psi_\beta \rangle$ is not too close to zero which would cause numerical instability. The dimension of the basis was between 100 (AL1 potential) and 140 (Bhaduri potential). Convergence of the energy of the T_{cc} tetraquark for three different runs of the code is shown in Fig.11. Here the asymptotic state of two free meson presents local minima toward which the results are converging at first. Only at sufficiently large number of basis states ($N > 70$) the bound state can be recognized. The initial parameters are always randomly chosen and then the optimization by Newton or simplex method is performed.

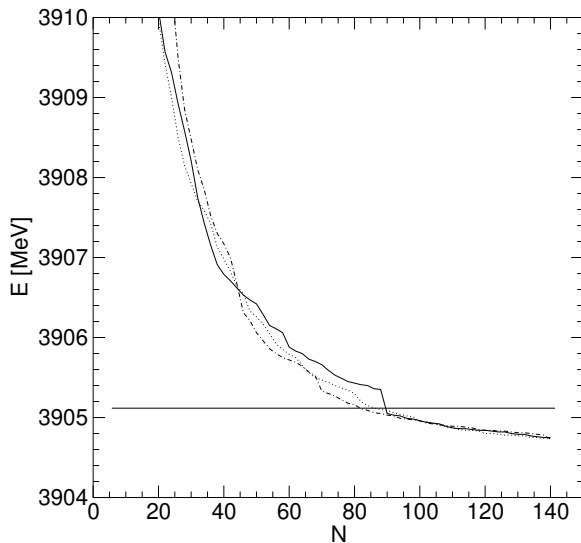


Figure 11: Energy of the T_{cc} tetraquark with Bhaduri potential as a function of the number of the basis states for three different runs. The $D + D^*$ threshold is also shown. Since the initial parameters are chosen randomly, the convergence is similar as with the stochastic variational approach.

References

- [1] D. Janc and M. Rosina, *Few-Body Systems* **31**, 1 (2001).
- [2] B. Silvestre-Brac and C. Semay, *Z. Phys.* **C57**, 273 (1993).
- [3] D. M. Brink and Fl. Stancu, *Phys. Rev.* **D57**, 6778 (1998).
- [4] R. K. Bhaduri, L. E. Cohler, Y. Nogami, *Nuovo Cim.* **A65**, 376 (1981).
- [5] B. Silvestre-Brac, *Few-Body Systems* **20**, 1 (1996).
- [6] L. Ya. Glozman, Z. Papp, W. Plessas, K. Varga, R. F. Wagenbrunn, *Nuc. Phys.* **A623** 90c (1997).
- [7] A. Del Fabbro and D. Treleani, *Phys. Rev.* **D63**, 057901 (2001).
- [8] D. Janc, M. Rosina, D. Treleani, A. Del Fabbro, *Few-Body System Suppl.* **14** 25 (2002).
- [9] M. Mattson em et al., (SELEX Collaboration), *Phys. Rev. Lett.* **89**, 112001 (2002).
- [10] T. Affolder *et al.*, (CDF Collaboration) *Phys. Rev. Lett.* **84**, 1663 (2000).

- [11] M. Rosina and D. Janc, *Bled Workshop in Physics* **4**, No.1,103 (2003).
- [12] J. Schaffner-Bielich and A. P. Vischer, *Phys. Rev.* **D57**, 4142 (1998).
- [13] M. Beneke and G. Buchala, *Phys. Rev.* **D53** 4991 (1996).
- [14] V. Dmitrasinovic, *Phys. Lett.* **B499**, 135 (2001).
- [15] V. Dmitrasinovic, *Phys. Rev.* **D67**, 114007 (2003).
- [16] S. Pepin and Fl. Stancu, *Phys. Rev.* **D65**, 054032 (2002).
- [17] K. Abe *et al.*, (Belle Collaboration), *Phys. Rev. Lett.* **89**, 142001 (2002).
- [18] K. Hagiwara *et al.* (Particle Data Group). *Phys. Rev.* **D66** 010001 (2002).
- [19] Y. Suzuki and K. Varga, *Stochastic Variational Approach to Quantum-Mechanical Few-Body Problems*, Springer-Verlag Berlin Heidelberg (1998).